Spin selectivity in the ultraviolet photodissociation of phosgene

Christof Maul, Tobias Haas, Karl-Heinz Gericke, and Franz Josef Comes
Institut für Physikalische und Theoretische Chemie, der Johann Wolfgang Goethe-Universität, Marie Curie-Strasse 11, 60439 Frankfurt am Main, Germany

(Received 28 June 1994; accepted 19 October 1994)

The ultraviolet photodissociation of phosgene in its first absorption band $^1A_2 \leftarrow {}^1A_1$ was investigated by resonance enhanced multiphoton ionization and time of flight techniques. Nascent atomic chlorine fragments were observed and their state specific kinetic energy distributions were determined. Of the chlorine atoms 15% are produced in the excited $^2P_{1/2}$ spin–orbit state with a mean kinetic energy of 3200 cm^{-1} compared to a value of 1500 cm^{-1} for the mean kinetic energy of the ground state chlorine atoms. The analysis of the kinetic energy spectra yielded evidence for a concerted three-body decay. The formation of intermediate COCl is of minor importance in the dissociation process, the formation of a stable final COCl product can be excluded. Competing pathways on the upper potential energy surface are discussed. A significant excitation of the carbon monoxide CO fragments is predicted.

I. INTRODUCTION

Determining product state distributions, translational energy distributions, and vector correlations among directed quantities of nascent reaction products serve as experimental tools for understanding the mechanism of a chemical transformation. In cases where fragments with unpaired electrons are generated, additional sources of information are spin–orbit state distributions and, if nonzero orbital angular momentum is involved, Λ sublevel distributions, and the respective state specific kinetic energy distributions.

Whereas in numerous cases Λ state distributions[1] have successfully been exploited for determining the spatial alignment of the electronic wave functions, hence for characterizing the geometric constraints of the dissociation process, relatively little is known about the mechanisms leading to nonstatistical spin–orbit state distributions or spin state specific translational energy spectra.

Photofragment translational spectroscopy (PTS)[2,3] allows the determination of the energy partitioning among the fragments of a dissociating system, and in favorable cases also conclusions on the dissociation mechanism. Drawbacks in the standard PTS experiment are its nonsensitivity towards slow particles that do not hit the particle detector within a sensible period of time, and its inability to discriminate against different fragment internal states when electron impact or nonresonant multiphoton processes are employed in the fragment ionization.

In this paper we present results obtained with a modified PTS experiment which overcomes those limitations and allows to state specifically obtain the complete kinetic energy spectrum. We have investigated the uv photodissociation of phosgene ($COCl_2$) by monitoring the state specific translational energy spectra of atomic chlorine fragments. The $COCl_2$ photodissociation is an excellent example for demonstrating the power of the modified PTS experiment because both spin polarization and spin-selective fragment translational energy distributions are important features of the process. Special emphasis is laid on the question whether the dissociation proceeds stepwise or concerted, synchroneous or nonsynchroneous.[4–8] Consequences for the energy transfer into the CO fragments are discussed.

The ground state phosgene $\tilde{X}\ ^1A_1$ is planar and belongs to the point group C_{2v}.[9] It exhibits a relatively weak absorption continuum between 215 and 305 nm with an oscillator strength $f = 1.04 \cdot 10^{-3}$ which has been assigned to the dipole-forbidden $\pi^* \leftarrow n$, $^1A_2 \leftarrow {}^1A_1$ transition. In contrast to the corresponding transition in H_2CO only a weakly pronounced structuring due to different vibrational transitions has been observed whereas the vibronic bands themselves remain featureless.[10] While the H_2CO photodissociation has intensely been studied and is very well characterized today,[11,12] surprisingly little is known about the products and about pathways of the photodissociation of phosgene although this process is considered to be its dominant sink in the stratosphere.[13,14]

Previous studies[15,16] led to the proposition of a sequential decomposition mechanism via formation of the thermally instable chloroformyl (ClCO) radical with immediate subsequent decay into CO and Cl agreeing well with the observation of the CO quantum yield being unity at 253.7 nm.[17] However, to our knowledge the first direct observation of atomic chlorine from the photodissociation of phosgene has only very recently been published at a dissociation wavelength of 248 nm.[18] The fraction of chlorine in the upper $^2P_{1/2}$ spin state (Cl*) was below the detection limit of 5%.

II. EXPERIMENT

The experimental setup[19] consists of a home-built single-field time-of-flight (TOF) spectrometer with a ratio of the acceleration region to the drift region of 1:2. The spectrometer was evacuated to a base pressure of 10^{-4} Pa (10^{-6} mbar) by two turbomolecular pumps. Pure phosgene (Messer Griesheim) without further purification was jet cooled and fed into the spectrometer via a pulsed nozzle (General Valve). The nozzle diameter was 0.5 mm, and the valve was operated at a stagnation pressure of $3 \cdot 10^4$ Pa and a pulse duration of 250 μs. Typical background pressures with the nozzle in operation were in the order of 10^{-3} Pa at a repetition rate of 10 Hz.

 0021-9606/95/102(8)/3238/10/$6.00

Simultaneous dissociation of phosgene and state-selective detection of chlorine atoms was performed using a single dye laser pumped by an excimer laser (Lambda Physik LPD 3000, Lambda Physik LPX 605i). The dye laser was operated with Coumarin 47 at a repetition rate of 10 Hz, its light was frequency doubled by a BBO crystal and focussed into the spectrometer by a 60 mm quartz lens. It intersected the molecular beam at an angle of 54° while the spectrometer axis formed a 90° angle with the propagation direction of the laser beam. The angle between the spectrometer axis and the electric field vector of the linearly polarized laser beam could be varied from 0° to 90° in order to investigate the spatial fragment distribution. The intensity of the laser light and the particle density in the gas pulse were carefully controlled in order to avoid kinetic energy transfer onto the fragments due to space charge effects. The laser intensity was typically kept below 500 μJ per pulse. The particle density in the supersonic beam has been varied in order to investigate the space charge induced distortion of the time-of-flight profiles and was kept well below the onset of Coulomb distortion for the actual measurements.

Electronically excited atomic chlorine was resonantly ionized employing a (2+1)-REMPI (resonance enhanced multiphoton ionization) scheme via the $4p^2D^0_{3/2} \leftarrow 3p^2P_{1/2}$ transition at 237.808 nm, respectively, the $4p^2P^0_{1/2} \leftarrow 3p^2P_{1/2}$ transition at 235.205 nm, ground state atomic chlorine was monitored via the $4p^2D^0_{3/2} \leftarrow 3p^2P_{3/2}$ transition at 235.336 nm.[20] The ions were detected by a double stage multichannel plate assembly (Galileo) with 40 mm active diameter.

The experimental performance was greatly enhanced by operating the system in two different modes: (a) the drift mode and (b) the acceleration mode.

In the drift mode no acceleration field was applied, so the spectrometer consisted simply of a 57 cm long drift tube. After passing a discriminator (FAST 7011) the ion signal was monitored by a multihit time-to-digital converter (FAST 7885) with a time resolution which could be set from 5 to 80 ns per channel, and stored in a data buffer (FAST MCD/PC). Typical acquisition times for a single spectrum were 3000 s with a total of $3 \cdot 10^5$ counts. For calibrating the conversion of time-of-flight profiles into translational energy spectra the Cl atom signal from the 308 nm photodissociation of molecular chlorine was monitored.

In the acceleration mode the ions were accelerated by a static electric field (typically 1000 V/m) in the acceleration region and detected after passing the drift tube. The ion signal was monitored by a digital transient wave form recorder (LeCroy 9450). The correctness for of Eq. (1) for calculating the initial particle velocities from the observed time-of-flight profiles has been proven by a set of calibration molecules with well-characterized energy partitioning. Since the experimental accuracy is much higher in the drift mode, calibration was performed against the drift data, which in turn were calibrated by investigating the dissociation of molecular chlorine at 308 nm (cf. Sec. IV B). Moreover, it was carefully checked that acceleration data from varied acceleration conditions yielded identical results.

In both acquisition modes, immediately after each time-of-flight profile a second profile was monitored with the laser delayed with respect to the gas pulse by 1 ms under otherwise identical conditions. This background signal contained the contribution of particles with a different charge-to-mass ratio, since no mass filter was employed in our spectrometer, and of parent molecules that had been fed into the spectrometer in a preceding nozzle pulse and were thermalized by collisions with the spectrometer walls. The background signal was then subtracted from the previously obtained time-of-flight profile in order to obtain the signal that is generated by the dissociation of jet-cooled phosgene alone. Further data processing was performed by a standard personal computer.

III. DATA EVALUATION

The conversion of time-of-flight drift profiles into kinetic energy distributions is straightforward due to the simple relationship between the fragment velocity v and the time of flight t for a given spectrometer length $s: v = s/t$. The general mathematical conversion procedure is described in the Appendix.

However, in interpreting data that are derived from drift measurements only one might be missing important information about the process one wants to study, since the drift mode is insensitive to slow particles. In order to detect also particles with low kinetic energy one has to apply an accelerating voltage. Therefore the procedure of converting time of flight profiles into kinetic energy spectra as described in the Appendix has to be modified following the considerations below.

The initial kinetic energy E of a particle leads to a broadening of the mass peak which in usual mass spectrometry one seeks to compensate for by realizing energy focusing conditions. The kinetic energy spectrometer, however, has been designed for a large energy dispersion dt/dE which increases energy resolution by giving up high mass resolution. The 1:2 geometry of the spectrometer guarantees a linear relationship between the width t of a time of flight acceleration profile (defined as the temporal deviation from the mass peak center t_0) and the initial fragment velocity v_x along the spectrometer axis. A simple calculation yields

$$v_x = \frac{8st}{3t_0^2}. \tag{1}$$

To begin with let us consider the case of an infinitely small detector. Only particles with an initial velocity $v = v_x$ will be detected because any nonzero velocity component apart from v_x will cause the particle to miss the detector—an effect that is commonly referred to as ion fly out. In this case from the considerations in the Appendix we find that $f_v(v) \sim f_t(t)$ and $f_E(E) \sim f_v(v)/v \sim f_t(t)/t$ due to the linear relationship between t and $v_x = v$.

In contrast, the relation between $f_v(v)$ and $f_t(t)$ in the case of an infinitely large flat detector is given by

$$f_t(t) = \int_{v_x(t)}^{\infty} f_v(v)/v \; dv, \tag{2a}$$

$$f_v(v) = v \cdot \frac{d}{dv}[f_t(t)] = t \cdot \frac{d}{dt}[f_t(t)]. \tag{2b}$$

In reality, where one has to deal with the intermediate case of a finite size detector of radius r_D a time of flight deviation t from the line center will be caused by all particles that have an initial velocity v between a lower limit $v_x(t) = 8st/3t_0^2$ [Eq. (1)] and an upper limit $v_u(t) = \sqrt{v_x^2 + (r_D/t)^2}$ above which ion fly out occurs. Thus $f_t(t)$ is given by

$$f_t(t) = \int_{v_x(t)}^{v_u(t)} f_v(v)/v \; dv, \tag{3a}$$

$$f_v(v) = f_v(v_u) \cdot (v/v_u)^2 - t \cdot \frac{d}{dt}[f_t(t)]. \tag{3b}$$

The latter equation can only be solved iteratively, because calculating f_v for a certain value of v requires the knowledge of f_v at $v = v_u(v)$. The starting point is the velocity distribution $f_{v,0}(v)$ with complete neglect of fly out: $f_{v,0} = t \cdot (d/dt)[f_t(t)]$. Inserting $f_{v,0}(v_u)$ into Eq. (3) one obtains the first iteration $f_{v,1}(v) = f_{v,0}(v_u) \cdot (v/v_u)^2 - t \cdot (d/dt)[f_t(t)]$. Consequently applying this scheme yields $f_{v,n}(v) = f_{v,n-1}(v_u) \cdot (v/v_u)^2 - t \cdot (d/dt)[f_t(t)]$ which rapidly converges to $f_v(v)$. The kinetic energy spectrum is then calculated by $f_E(E) = f_v(v) \cdot (dv/dE) \sim f_v(v) \cdot v$.

In the case of acceleration profiles the velocity v_{beam} of the molecular beam does not change the deviation Δt from the center of the time-of-flight profile t_0—which is the directly measured quantity in the acceleration mode. However, there is a small influence on the rate of ion fly out, and hence for the shape of the corresponding time-of-flight profile, when observing a single fragment velocity v only. Not only being small in the beginning, this effect is almost completely cancelled out for observing a velocity distribution $f(v)$. For those reasons it is not necessary to perform a transformation from the laboratory to the center of mass coordinates for the evaluation of acceleration profiles. In contrast, for drift measurements the time of flight t_0 itself is the directly measured quantity, so the transformation from laboratory to center-of-mass coordinates described in the Appendix must be performed.

In order to assure the correctness of the above described procedure the drift experiment is performed for the dissociation of a molecule with a well-characterized energy partitioning, preferably with a mass equal or at least similar to the mass under investigation. This allows to rule out perturbations by electric stray fields inside the spectrometer and to determine the exact distance between laser beam focus and detector position. It also serves as a basis to correctly interpret the acceleration profiles that are inherently less accurate with respect to energy resolution due to the comparatively large influence of the spectrometer response function with a width of approximately 50 ns.

The method as described above is applicable to spatially isotropic product distributions. Any anisotropy must explicitly be accounted for by modifying the evaluation procedure accordingly.

If the overall time of flight t_0 of the accelerated species is chosen to be large enough, one needs not to worry about errors induced by narrow band excitation of the products by a laser the spectral bandwidth of which is less than the product Doppler width. The condition that must be satisfied is that the off-axis velocity v_z (z being perpendicular to the spectrometer axis) is large enough in order for ion-fly out to occur, i.e.,

$$v_z = c \cdot \frac{\Delta \nu}{\nu_0} \, l > r_D/t_0, \tag{4}$$

where r_D is the detector radius, c is the speed of light, and ν_0 and $\Delta \nu_l$ are the frequency center and the bandwidth of the laser.

When care is taken that the aforementioned limitations are observed, the evaluation procedure assures the monitoring of all kinetic energies E including $E = 0$ in the determination of the kinetic energy spectrum and at the same time exploits the high accuracy of the standard photofragment translational energy (PTS) measurements. The shape of the energy distribution is determined by the acceleration profiles only. The high energy portions of the distributions that are obtained from drift, respectively, from acceleration profiles are identical whereas the drift profiles contain no or misleading information about the low energy portion. In contrast, the energy resolution is governed by the width of the response function of the apparatus in the drift mode. It must be determined separately for each species by monitoring well-characterized, monoenergetic calibration fragments, such as, e.g., Cl atoms from Cl_2 dissociation or H atoms from HI dissociation.

IV. RESULTS

A. Mass spectra

In a time-of-flight mass spectrum obtained with nonresonant multiphoton excitation of phosgene and phosgene fragments at $\lambda = 235.10$ nm under strong acceleration conditions we observed the peaks for a mass to charge ratio of 28 and 35/37 indicating the presence of CO^+ and Cl^+. The intensity ratio for the mass to charge ratios 35 and 37 is 3:1 which reflects the natural occurrence of the chlorine isotopes. No mass peaks have been observed for $m/e = 63/65$ and 70/72/74 corresponding to $COCl^+$ or Cl_2^+. This lets us conclude that C–Cl bond fission is the dominant process in the dissociation of phosgene at 235 nm.

B. Drift mode calibration

Molecular chlorine was photodissociated at 308 nm in order to investigate the accuracy of the spectrometer in the appropriate time of flight regime. The dissociation at this wavelength is well characterized and is known to almost exclusively yield atomic chlorine fragments in the $^2P_{3/2}$ ground state.[21,22] The calibration profile is depicted in the bottom part of Fig. 1. The Cl atom velocity is calculated to be 2060 m/s from the difference of the photon energy and the dissociation energy of $E_{\text{diss}}(Cl_2) = 20\,000\ \text{cm}^{-1}$. The Cl atom time of flight profile is best reproduced by convoluting the four possible arrival times that are due to the isotopic composition of Cl_2 with a Gaussian shaped response function with a width of 7 μs. Taking into account the center of mass

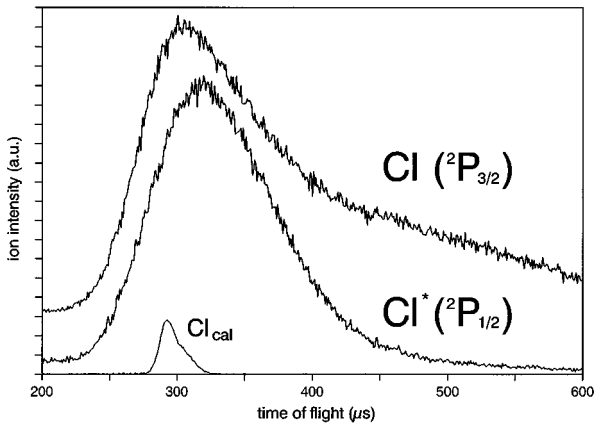

FIG. 1. TOF profiles observed in the drift mode. The upper two traces result from the photodissociation of phosgene while the lower trace (Cl_{cal}) is a calibration profile from the 308 nm dissociation of molecular Cl_2 that is known to produce monoenergetic ground state Cl only. The asymmetry of this calibration profile is due to the isotopic distribution of chlorine. All traces are corrected for background signal and normalized with respect to peak height. Note that ground state Cl($^2P_{3/2}$) peaks at lower TOF (corresponding to higher kinetic energy) than the excited state Cl*($^2P_{1/2}$) due to the lack of internal excitation of the chlorine atom and the shorter dissociation wavelength, but has a pronounced tail at low kinetic energy.

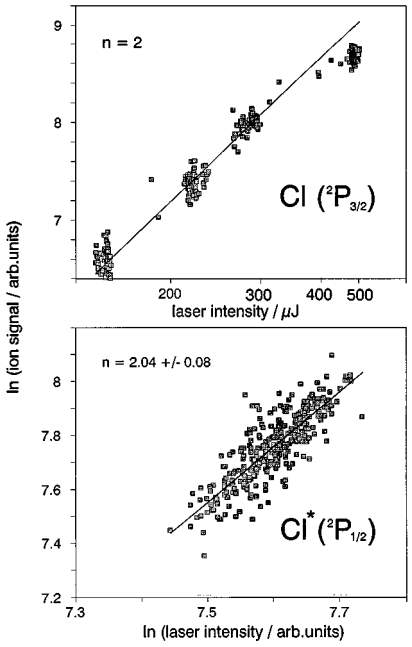

FIG. 2. Log–log plots of the dependence of the REMPI signal intensity on the applied laser intensity. The data have been acquired by monitoring the signal and laser intensities caused by shot-to-shot fluctuations of the laser power at the center of the Doppler broadened resonance transitions for the respective spin–orbit states. In the upper panel the pulse energy has been varied from 125 to 500 mJ. The straight line represents a quadratic dependence of the REMPI signal on the laser intensity. For high pulse energies a deviation from quadratic behavior can be seen which is caused by partly saturating the two-photon resonance step. For very low pulse energies noise is the dominant feature due to very low signal intensity. In the lower panel the power dependence for intermediate pulse energies as were typically employed in the experiment is shown on an enlarged scale. The straight line with slope 2 is yielded from a linear regression procedure.

motion of the molecular beam the expected time of flight value for the $^{35}Cl^{35}Cl$ dissociation calculated from the spectrometer geometry is 285 μs. This value lies within the width of the response function of the observed flight times. This excellent agreement eliminates the need for correcting our experimental data for stray field perturbations. The velocity resolution $\Delta v/v$ is calculated to be 2.5% corresponding to a kinetic energy resolution of 5%.

C. Spin component population ratio

In total four photons are involved in the formation of an ion signal: one for dissociating $COCl_2$, two for the resonant transition to the intermediate state, and one for ionizing the Cl atom. The intensity of the ion signal S from the dissociation of phosgene on the laser power I_L for the transitions with the $^2D^0_{3/2}$ state as resonant intermediate is depicted in Fig. 2 for single shot events. Linear regression yielded a quadratic relationship

$$S \simeq I_L^n \quad \text{with} \quad \begin{matrix} n_{\mathrm{Cl}} = 2.09 \pm 0.09, \\ n_{\mathrm{Cl}^*} = 2.04 \pm 0.08. \end{matrix}$$

The photon flux in the focus is calculated to be approximately 10^{19} photons/cm^2 per pulse with a focus diameter of 50 μm and a laser intensity of 200 μJ. The dissociation step is therefore saturated as can be deduced from comparing the photon flux value with the phosgene absorption cross section of $\sigma = 1.8 \cdot 10^{-19}$ cm^2 at 235 nm[10]. The saturation behavior of the detection scheme can only qualitatively be discussed because neither the transition probabilities for the two-photon excitation step nor for the ionization step from the $^2D_{3/2}$ state to the ionization continuum are known. However, the efficiency for the ionization step is by orders of magnitude larger due to its one-photon character than for the two-photon resonant transition. Therefore, the ionization step is more easily saturated than the two-photon excitation, and from the quadratic dependence of the signal intensity on the laser intensity we conclude that the dissociation step as well as the ionization step are essentially saturated whereas the two-photon resonant transition is not. The experimental conditions are similar to those of Matsumi *et al.*[21,23] who determined a ratio of the transition probabilities B of $B(\mathrm{Cl}^*)/B(\mathrm{Cl}) = 0.4$.

Scanning the laser over the two resonance transitions yielded the Doppler profiles of Fig. 3. Integrating the area S under the profiles resulted in a signal ratio $S(\mathrm{Cl}^*)/S(\mathrm{Cl})$ of 0.07. Taking into account the transition probabilities B we determined a Cl* yield $\phi(\mathrm{Cl}^*) = 0.15$ where ϕ is defined as the ratio of the number of excited state atoms $P(\mathrm{Cl}^*)$ to the total number of chlorine atoms: $\phi(\mathrm{Cl}^*) = P(\mathrm{Cl}^*)/[P(\mathrm{Cl}) + P(\mathrm{Cl}^*)]$.

D. Kinetic energy distributions

Time of flight profiles of Cl and Cl* products obtained in the acceleration mode are shown in Fig. 4 where the Cl* fragments carry an additional amount of $\Delta E(^2P_{1/2} - {}^2P_{3/2}) = 882$ cm^{-1} of internal energy. The transients of Fig. 4 consist of the mass to charge ratios $m/e = 35$

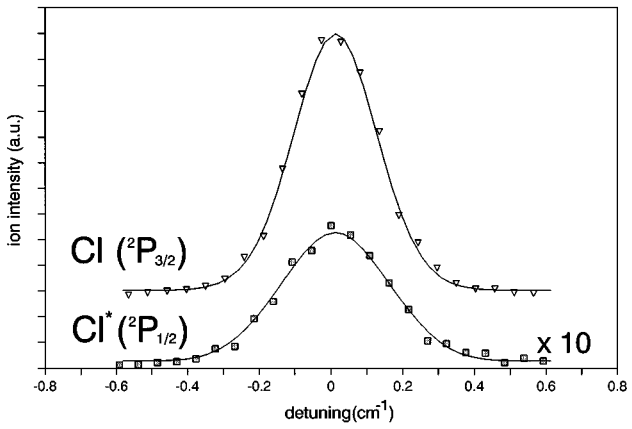

FIG. 3. Doppler profiles of the $4p^2D^0_{3/2} \leftarrow 3p^2P_{1/2}$ transition at 237.808 nm and the $4p^2P^0_{1/2} \leftarrow 3p^2P_{1/2}$ transition at 235.205 nm, obtained by scanning the probe laser over the resonances. Symbols mark experimental data, each of which is averaged over 20 laser shots. Solid lines are Doppler profiles that have been calculated from the kinetic energy distributions of Fig. 1 that were obtained from the TOF data with the evaluation procedure described in Sec. III. The lower trace of Cl*($^2P_{1/2}$) has been magnified by a factor of 10.

and $m/e=37$ which are broadened by the initial kinetic energy of the fragments. The width of the mass peaks is proportional to the fragment velocity component v_x along the spectrometer axis. A remarkably different behavior of the two spin components with respect to their kinetic energy acquisition in the photodissociation is obvious. The effect is large enough for the two isotopes of Cl* to exhibit overlapping time-of-flight profiles while the two masses for ground state Cl atoms are still clearly separated from one another. The reason for this overlap is that the time until arrival at the detector for those ^{37}Cl fragments initially flying towards the detector equals the time of flight for those ^{35}Cl fragments initially flying away from the detector which have to turn around in a time consuming process before finally approaching the detector. The individual contributions of the two Cl isotopes are shown in the upper panel of Fig. 4. They have been calculated from the respective undisturbed parts of the TOF shapes where the signals do not overlap, i.e., from forward flying ions for ^{35}Cl and from backward flying ions for ^{37}Cl. This procedure gives rise to slightly different shapes reflecting a higher resolution of the spectrometer for backward flying particles. Apart from determining the energy resolution of the distributions calculated below from the experimental data, this does not influence the further data evaluation, and all conclusions drawn below have been derived from the TOF shape of the ^{35}Cl isotope.

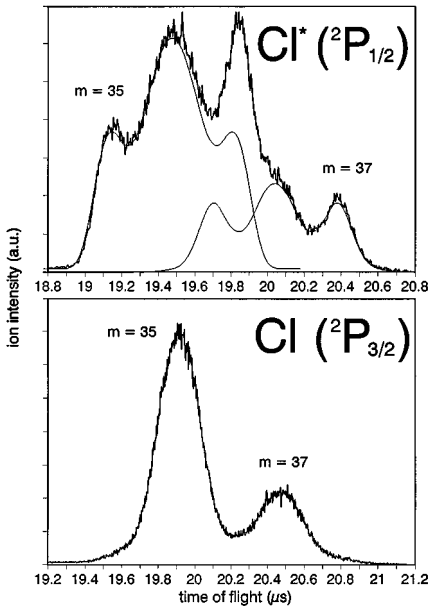

FIG. 4. TOF profiles observed in the acceleration mode. Each transient is contributed to by both Cl isotopes ^{35}Cl and ^{37}Cl with their natural isotope ratio of 3:1. The average has been taken for 1000 laser shots, the peak height has been normalized. Note the overlap of the two isotopes for Cl*($^2P_{1/2}$) in the upper panel due to identical TOF for backward flying ^{35}Cl and for forward flying ^{37}Cl. The slightly different shapes of the two calculated individual contributions of the two isotopes are due to a higher energy resolution of the spectrometer for backward flying particles as compared to the resolution for forward flying particles.

In a one-color experiment monitoring different spin–orbit states goes inevitably along with a variation in dissociation wavelength. For example, in the H_2CO photodissociation a dependence of the rotational state distribution on the dissociation wavelength has been monitored.[11,12] Therefore, this effect cannot *a priori* be ruled out in the case of phosgene although the structures in the phosgene absorption spectrum are by far not as pronounced as for formaldehyde. In order to confirm that the observed effect is solely due to the spin–orbit state that is being monitored and not to the variation in dissociation energy additional time of flight profiles for Cl* were obtained with the $^2P^0_{1/2}$ state as resonant intermediate at 235.205 nm instead of the $^2D^0_{3/2}$ state at 237.808 nm. Since the Cl* profiles obtained with different intermediate states are indistinguishable from one another, spin selective energy partitioning is indeed taking place: Cl in the electronic ground state is preferentially produced with low kinetic energy whereas Cl* in the excited spin–orbit state is preferentially produced with large kinetic energy.

The high energy portion of the velocity distribution can to a much higher degree of accuracy be measured in the drift mode. The observed drift profiles for the two spin–orbit states are shown in Fig. 1 after having been normalized to each other with respect to peak height and corrected for minor background signal (cf. Sec. II). The drift profiles for the two spin–orbit states are by far not as distinguishable from one another as the corresponding acceleration profiles are, although a tendency of the ground state Cl for having lower kinetic energy is clearly visible. The reason for this is that whereas the accuracy of drift profiles for the high energy portion of the translational energy distribution is much higher than that of the acceleration profiles the drift mode is insensitive to particles with velocities below 1000 m/s. This is due (a) to the fact that the molecular beam traverses the spectrometer perpendicularly carrying slow particles away and (b) to the decrease in detection efficiency for a very large time of flight ($t \geqslant 1$ ms). For the dissociation of phosgene neglecting the products with low kinetic energy that are invisible in the drift measurements would have dramatic con-

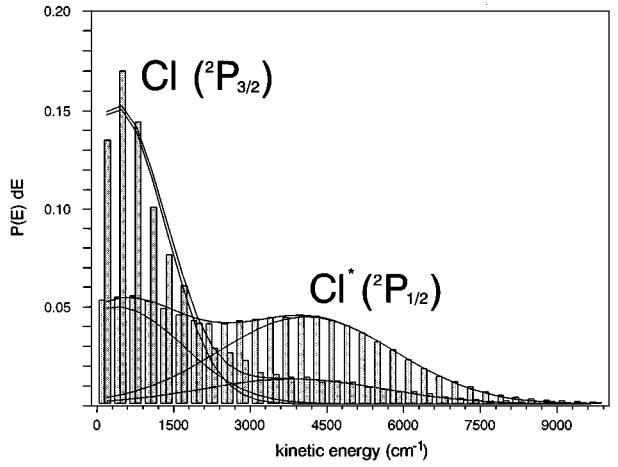

FIG. 5. Kinetic energy spectra obtained from the combined drift and acceleration TOF profiles. Areas have been normalized in order to stress the difference in the kinetic energy distributions, and do not reflect the spin state population ratio. These distributions form the basis for calculating the Doppler profiles of Fig. 3. The solid lines describe the best fit of two Gaussian shaped distribution to each of the bimodal kinetic energy distributions of Cl and Cl*, respectively. The sum of the corresponding distributions is shown as well as the respective distributions for the low and the high energy components.

sequences for the data evaluation because those fragments carry the most information due to their pronounced spin-selective behavior.

An appropriate method to overcome these limitations is described in Sec. III. The state specific kinetic energy spectra obtained with this method are shown in Fig. 5. The state specific mean kinetic energies are extracted to be $E[\mathrm{Cl}(^2P_{3/2})]=1500\ \mathrm{cm}^{-1}$ and $E[\mathrm{Cl}^*(^2P_{1/2})]=3200\ \mathrm{cm}^{-1}$, respectively, with an upper limit of 5% for the experimental error in the kinetic energy that is estimated from the drift mode response function. A bimodal kinetic energy distribution, which is obvious for the excited spin–orbit state, also is appropriate in order to describe the ground state kinetic energy spectrum which at first glance consists of a single peak at low kinetic energy with a high energy tail attached to it. Each of the translational energy spectra can be fitted by the sum of two Gaussian shaped distributions, one of which is centered around 350 cm^{-1} (low energy component) while the other one (high energy component) is centered around 3850 cm^{-1} for ground state Cl and around 4000 cm^{-1} for excited state Cl*. The results of the fit procedure are shown in Fig. 5. The fit parameters are listed in Table I. The accuracy of the obtained values for the individual contribution is better than 20%. Considering the $\mathrm{Cl}^*(^2P_{1/2})$ yield of 0.15 (cf. Sec. IV C) we find a 0.71 contribution of the low energy component of ground state $\mathrm{Cl}(^2P_{3/2})$ and only a 0.04 contribution of the low energy component of excited state $\mathrm{Cl}^*(^2P_{1/2})$. The contribution of the high energy component is 0.11 for Cl* and 0.14 for ground state Cl. Therefore, the bimodal structures can be described as a 0.25 contribution of the high energy distribution with a $0.11{:}0.14 \approx 1{:}1.3 \pm 0.3$ ratio of Cl*/Cl generation, and a 0.75 contribution of the low energy distribution with a Cl*/Cl generation of $0.04{:}0.71 \approx 1{:}18 \pm 5$.

TABLE I. Fit parameters for the low and high energy components of ground state $\mathrm{Cl}(^2P_{3/2})$ and excited state $\mathrm{Cl}^*(^2P_{1/2})$. Given are contributions A, centers E_0, widths ΔE (FWHM), and mean kinetic energies E for each component separately and summed up for the individual spin–orbit states. All energies are in cm^{-1}. The difference between the values for the center E_0 of the distribution and the mean kinetic energy E is due to the large width of the distribution that is cut off at $E=0$.

	Cl*(slow)	Cl*(fast)	Cl(slow)	Cl(fast)	Cl*	Cl
A	4%	11%	71%	14%	15%	85%
E_0	350	4000	350	3850		
ΔE	1600	2600	1380	2500		
E_{fit}	1040	4070	920	3910	3190	1430
E_{exp}					3170	1520

Implications of the bimodal distributions will be discussed in the following section.

The high quality of the evaluation procedure is demonstrated by comparing the experimentally observed Doppler profiles of Fig. 3 (data points) that had originally been observed in order to determine the population ratio of the two spin–orbit states to Doppler profiles (solid lines) that are calculated from the energy distributions obtained with the evaluation procedure described in the preceding chapter. The agreement of the calculated profiles with the experimental data in Fig. 3 is excellent.

The evaluation procedures for obtaining kinetic energy distributions from the experimental data and for calculating Doppler profiles from the kinetic energy distributions use the assumption of spatially isotropic fragment distributions. In order to examine the correctness of this assumption all TOF experiments—acquisition of acceleration and drift profiles—have been performed with polarization angles of 0° and 90°. Neither changes in the amplitude nor in the shape of the observed profiles could be observed, so assuming an isotropic fragment distribution is justified in the evaluation procedure. The experimental setup as a one-color experiment does not allow to vary the polarization direction between dissociating and analysing laser light. Only the $\langle \boldsymbol{\mu} \cdot \mathbf{v} \rangle$ correlation between the transition moment $\boldsymbol{\mu}$ and the spatial distribution of the fragments, characterized by the preferred direction of the velocity $\mathbf{v}$, can therefore be determined.[24] For atomic fragments, however, this limitation is insignificant.

V. DISCUSSION

A. Dissociation mechanism

From the kinetic energy distributions we conclude that no two-photon dissociation of phosgene occurs under our experimental conditions. For a two-photon process the additional deposition of another uv photon carrying 42 500 cm^{-1} of energy before the fragmentation takes place would not be sufficient to generate electronically excited fragments other than those observed. The additional available energy would accordingly have to be channeled into fragment kinetic energy essentially. The resulting two-photon available energy $E_{\mathrm{av}(2)}=58\,000\ \mathrm{cm}^{-1}$ would lead to a minimum kinetic energy of 8 500 cm^{-1} per chlorine atom in the case of the dissociation of a ''degenerate'' linear $COCl_2$ parent molecule

which is much higher than the observed kinetic energy. Any realistic parent molecule geometry would yield even higher kinetic energy values for the fragments.

The one-photon dissociation of phosgene can in principle proceed along one or several of the following pathways. Listed below are those dissociation channels which are energetically accessible at a dissociation wavelength of 235 nm

$$COCl_2 + h\nu \rightarrow COCl + Cl/Cl^*, \tag{5}$$

$$COCl_2 + h\nu \rightarrow COCl^* + Cl/Cl^* \rightarrow CO + Cl + Cl/Cl^*, \tag{6}$$

$$COCl_2 + h\nu \rightarrow CO + 2\ Cl/Cl^*, \tag{7}$$

$$COCl_2 + h\nu \rightarrow CO + Cl_2. \tag{8}$$

Reaction (5) yields a stable chloroformyl radical and a chlorine atom as products. We will call this pathway the radical channel. Process (6) is a fragmentation that proceeds in two independent steps. The first one yields identical products as reaction (5) does, but the chloroformyl radical which is excited above the dissociation energy decays in a second step to a CO molecule and a second atomic chlorine fragment. This pathway is called the sequential mechanism. Reaction (7) yields a CO molecule and two atomic chlorine fragments in a single step and is therefore called three-body decay. This mechanism might further be characterized by determining whether the bond cleavages occur simultaneously, giving rise to Cl atoms with identical energy content, or nonsimultaneously, but nevertheless in a concerted manner, yielding Cl atoms with different energy contents. The latter case might be imagined, e.g., as a parent molecule breaking apart out of an asymmetric stretching mode while the former might be realized by a fragmentation out of a symmetric stretching mode. Finally, reaction (8) yields two molecular products: A CO molecule and a Cl_2 molecule. This pathway requires a complex electron rearrangement by forming a new Cl–Cl bond simultaneously to breaking the two C–Cl bonds. This mechanism will be called the molecular channel.

The molecular channel, of course, cannot be observed in our experiment. Whether it exists or not can only be decided by monitoring the energetics of the CO molecule or by direct observation of the molecular chlorine fragment as nascent particle. The further treatment will therefore be limited to discussing channels (5)–(7).

The value for the dissociation energy E_{Diss}(COCl–Cl) for dissociating phosgene into a chloroformyl radical, COCl, and one Cl atom is not explicitly found in the literature, but can be calculated as the difference of the dissociation energy E_{Diss}(Cl–CO–Cl)=28 700+/−240 cm^{-1},[9] required for the fragmentation of phosgene into a CO molecule and two chlorine atoms, and the dissociation energy E_{Diss}(CO–Cl)=2600+/−1200 cm^{-1} the chloroformyl radical.[25,26] From these values the dissociation energy E_{diss}(Cl–COCl) of phosgene for the formation of Cl and COCl and the available energy E_{av} to be distributed among the fragments are calculated to be

$$E_{\mathrm{Diss}}(\mathrm{Cl–COCl}) = 26100 +/- 1200\ \mathrm{cm}^{-1}, \tag{9}$$

$$E_{\mathrm{av}} = h \cdot \frac{c}{\lambda} - E_{\mathrm{diss}}(\mathrm{Cl–COCl}) = \begin{cases} 15\,900\ \mathrm{cm}^{-1}, & \lambda = 235.3\ \mathrm{nm} \\ 15\,500\ \mathrm{cm}^{-1}, & \lambda = 237.8\ \mathrm{nm} \end{cases}, \tag{10}$$

where λ is the dissociation wavelength, and h, c are Planck's constant and the speed of light, respectively.

From the following considerations we conclude that the radical channel (5) does not contribute to the fragmentation process of phosgene. If a stable COCl radical were generated in the dissociation together with an atomic Cl fragment this radical would have to carry an extremely low internal energy due to its very low dissociation energy. As a consequence the Cl atoms would have to be very fast possessing kinetic energies in the range from 8900 to 10 200 cm^{-1} for ground state Cl, and from 8000 to 9400 cm^{-1} for excited state Cl*. These values are calculated from the minimum and the maximum kinetic energies E_{min} and E_{max} that agree with the conservation of energy, $E_{\mathrm{min}} = E_{\mathrm{av}} - E_{\mathrm{Diss}}(\mathrm{COCl})$ and $E_{\mathrm{max}} = E_{\mathrm{av}}$, and from the conservation of linear momentum. Since no Cl atoms with this high kinetic energy are observed, the participation of the radical channel ($COCl_2 + h\nu \rightarrow COCl + Cl$) can be ruled out. We conclude therefore that every dissociation process produces two chlorine atoms and one carbon monoxide molecule. This is in accordance with measurements of Okabe who determined the quantum yield of CO formation to be unity at a dissociation wavelength of 253.8 nm.[17]

The question remains, however, whether the dissociation of $COCl_2$ into two Cl atoms and one CO molecule is a real three-body decay (7), i.e., if both C–Cl bonds break in a single event, or if the dissociation proceeds stepwise (6) as has previously been postulated.[15,16] The criterion for distinguishing between a concerted and a stepwise mechanism is if both bonds break within one rotational period of the parent molecule or if the parent molecule has enough time left after ejecting the first Cl atom to complete a full rotation before breaking apart into the final products.

Whereas in the first case there remains an angular correlation between the two Cl products, in the latter case the decay angle between the first and the second Cl atom underlies no restriction. An answer to this question is yielded by analyzing the translational energy spectra. In principle, the dissociation can proceed via different pathways even under identical conditions, e.g., some molecules might undergo a three-body decay while others might fragment in a sequential manner. If this were the case the resulting kinetic energy distribution would be composed of an energy distribution characteristic for a sequential decay mechanism and of another distribution reflecting the decay parameters of a concerted three-body decay. In the following we will determine an upper limit for the contribution of the sequential decay mechanism in order to show that the major dissociation mechanism is a concerted three-body decay where the two C–Cl bond cleavages occur within one rotational period of the parent molecule.

It has already been proven that the decay of ground state COCl yields ground state chlorine atoms only.[18] Therefore, the ground state Cl translational spectrum must contain the

information of a sequential decay if this process exists, and we will focus on the ground state kinetic energy distribution in order to determine the upper limit for the sequential mechanism. A sequential decay leads to a pronounced *symmetrically* double-peaked translational energy spectrum as has been shown by Lee and co-workers.[27] Whereas in our case both the translational energy spectrum of ground state $Cl(^2P_{3/2})$ as well as that of the excited spin–orbit state $Cl^*(^2P_{1/2})$ exhibit bimodal structures as was shown in Sec. IV D, they are not at all symmetric. Contributions to the high and low energy components of the relevant ground state kinetic energy spectrum differ by a factor $0.71:0.14 \simeq 5$. Thus the overwhelming part of the dissociation must proceed as a three-body decay. The maximum contribution of a sequential decay mechanism that cannot be ruled out by the experiment is determined if one assumes that every ground state chlorine atom belonging to the high energy component—accounting for 14% of the total amount of atomic chlorine—is generated via a sequential pathway. In this case an equal amount, i.e. another 14% of the total atomic chlorine, must be generated as low energy component. So at maximum 28% of all decay processes may proceed sequentially, whereas at least 72% must be characterized as three-body decays.

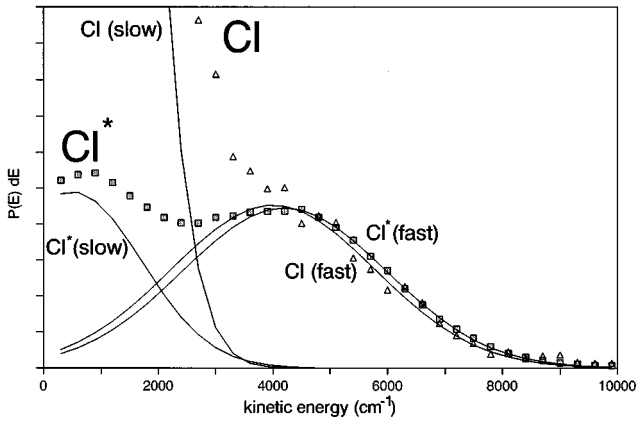

FIG. 6. Comparison of the fit results for the high energy components of ground and excited state Cl. The solid lines are the best fits for the respective components of the two spin–orbit states. The symbols mark experimentally observed data (triangles: Cl, squares: Cl*). In order to demonstrate the similarity of the high energy components, the peak heights for ground state $Cl(^2P_{3/2})$ and for excited state $Cl^*(^2P_{1/2})$ are normalized with respect to each other.

B. Spin polarization

The bimodal structures of the translational energy spectra can be interpreted as a 25% contribution of a high energy channel with a 1:1.3 ratio of Cl*/Cl generation, and an 75% contribution of a low energy channel with a Cl*/Cl generation of 1:18 (Table I and Sec. IV D). We postulate the existence of two different exit channels from the originally prepared excited state of the parent molecule, one leading to slow fragments, the other one leading to fast fragments. This view of the dissociation mechanism is supported—within the limits of the experimental error—by the equal amount of fast Cl and Cl* atoms and by the identical kinetic energy distributions for the high energy component of both spin–orbit states which are shown in Fig. 6. The high energy components of both states are likely to be generated by a process that is not sensitive to the spin–orbit state that is accessed in the dissociation. The low energy component, on the contrary, must accordingly be associated to a process that almost exclusively produces slow ground state chlorine atoms. A tentative assignment of these processes to the potential energy surfaces involved in the dissociation is discussed in the next section. Since no excited Cl* has been observed within the experimental uncertainty of 5% at a dissociation wavelength of 248 nm[18] we conclude that the high energy channel is not accessed at this wavelength and that the second exit channel from the upper potential energy surface is opened when changing the dissociation wavelength from 248 to 235 nm.

C. Electron configuration and intramolecular energy transfer

Phosgene is known to be predissociative in the excited electronic states. Indeed, the fact that the Cl products from the phosgene dissociation are distributed spatially isotropic means that the excited parent molecule has enough time left before breaking apart to complete at least half a rotation. From that we have determined a lower limit for the lifetime of the excited state of $\tau \geqslant 10$ ps. It is generally assumed that the original electronic excitation of phosgene into the $^1A_2$ state promotes a nonbonding electron to the antibonding $4b_1$ orbital which has π^*(C–O) character, thus weakening the CO double bond. Only slightly above this π^* orbital there lies the σ^*(C–Cl) orbital which finally leads to C–Cl bond cleavage. Thus an intramolecular energy transfer is likely to occur where energy of the parent molecule that has been excited into the $^1A_2$ state is transferred into the $^1B_2$ state which is repulsive in the C–Cl coordinate. Furthermore, a conversion of the electronically excited $^1A_2$ state to the $^1A_1$ ground state of phosgene may take place, in which the resulting high internal excitation governs the C–Cl bond cleavage. One might speculate that these two competing dissociation pathways are to be identified as the two exit channels that manifest themselves in the bimodality of the translational energy spectra. Within this interpretation the low energy atoms that leave a large internal excitation in the remaining CO molecule would be generated via the ground state potential energy surface while the high energy atoms would be correlated to a dissociation process via the electronically excited $^1B_2$ state producing relatively cold CO fragments.

From the arguments discussed in the preceding chapter we predict a significant internal excitation of the CO molecule since most Cl atoms (75%) are generated with low translational energy. Even if each high energy atom correlated with a low energy one—which is not necessarily the case—at least half of the dissociation processes would have to produce two low energy ground state Cl atoms with kinetic energies below 1200 cm^{-1} each. This sets an upper limit for the corresponding kinetic energy of the CO molecule of 6000 cm^{-1} due to conservation of linear momentum. This energy might be significantly lower, for there is no con-

straint on the recoil angles between the three fragments involved in the dissociation. This yields a lower limit for the internal energy $E_{\mathrm{int}}(\mathrm{CO})$, as defined by the difference between the available energy $E_{\mathrm{av}}=15\,900\ \mathrm{cm}^{-1}$ and the sum of the kinetic energies of all three fragments $E(\mathrm{Cl}-1)+E(\mathrm{Cl}-2)+E(\mathrm{CO})$ of

$$E_{\mathrm{int}}(\mathrm{CO})=E_{\mathrm{av}}-[E(\mathrm{Cl}-1)+E(\mathrm{Cl}-2)+E(\mathrm{CO})]$$
$$=15\ 900-8\ 400\ \ \mathrm{cm}^{-1}=7\,500\ \ \mathrm{cm}^{-1} \qquad (11)$$

for a significant amount of the CO fragments.

In order to obtain even more detailed knowledge about the $COCl_2$ system the next step to be taken is to monitor the CO fragment from the phosgene dissociation that has been proven to be present by our mass spectra. This can be done by using the $\tilde{B}\ ^1\Sigma^+$ state of CO as resonant intermediate with an excitation wavelength around 230 nm. This experiment is presently performed in our laboratory. Results will be published in a forthcoming paper.

VI. CONCLUSION

We report the direct observation of Cl atoms in the uv photodissociation of phosgene. Chlorine atoms are generated in the $^2P_{3/2}$ electronic ground state as well as in the electronically excited $^2P_{1/2}$ state. The process is highly spin selective, mean kinetic energies inferred in the Cl atoms differ by as much as 1700 cm^{-1} for the two spin–orbit states. The energy distribution proves the concerted three-body decay to be the major pathway in the process. The access of two competing exit channels from the upper potential energy surface is postulated. The formation of intermediate COCl is of minor importance in the dissociation process, the formation of a stable final COCl product can be excluded.

The power of combined drift and acceleration time of flight measurements together with a state selective detection scheme is demonstrated. The main features of the dissociation process—existence of two exit channels and concertedness—would not have been observed in a standard PTS experiment. Although far from being able to describe in complete detail such a complex process as phosgene dissociation involving not less than 48 electrons we have presented a technique that proves to be a valuable tool in investigating this kind of problems.

ACKNOWLEDGMENTS

We are greatly indebted to E. A. Reinsch who provided us with *ab initio* calculations on the phosgene molecule. Financial support by the Deutsche Forschungsgemeinschaft is gratefully acknowledged.

APPENDIX

Transforming time of flight profiles into velocity distributions resp. kinetic energy spectra is an example for the general problem of transforming a distribution f_x of a quantity x into a distribution f_y of a quantity y where $y(x)$ is a function of x. In general, the probability $f_y(y_0)$ to find a certain value y_0 for $y(x)$ is obtained by projecting all values of x with their respective weights $f_x(x)$ onto $y(x)$ under the condition that the value y_0 be realized for $y(x)$. If $y(x)$ is a monotoneous function of x this can be expressed by the following integral expression:

$$f_y(y_0)=\int dx\ f_x(x)\cdot\delta(y(x)-y_0). \qquad (A1)$$

The condition $y(x)=y_0$ is satisfied by introducing the delta function which in turn allows to simplify the integral by substituting x by y

$$f_y(y_0)=\int dy\ \frac{\partial x}{\partial y}(y)f_x(x(y))\,\delta(y(x)-y_0)$$
$$=\frac{\partial x}{\partial y}(y_0)f_x(x(y_0)). \qquad (A2)$$

Since this transformation can be performed for all values of y in the same way one might omit the subscript for y and one obtains the general relationship

$$f_y(y)=\frac{\partial x}{\partial y}(y)f_x(x(y)). \qquad (A3)$$

Applying this recipe to time of flight spectra yields the velocity distribution $f_v(v)$ and the translational energy spectrum $f_E(E)$

$$f_v(v)=\frac{\partial t}{\partial v}(v)f_t(t(v)), \qquad (A4a)$$

$$f_E(E)=\frac{\partial t}{\partial E}(E)f_t(t(E))=\frac{\partial v}{\partial E}(E)f_v(v(E)). \qquad (A4b)$$

from the experimentally observed time of flight profile $f_t(t)$. This transformation is easily obtained once the functional relations between t, v, and E are known.

For the drift experiments obtaining this relationship $v(t)$, respectively $E(t)$ is straightforward: The velocity component v_x along the spectrometer axis is given by the ratio of the total spectrometer length s to the total time of flight t: $v_x=s/t$. The particle velocity v in the laboratory frame is obtained by taking into account the center of mass velocity v_{beam} of the molecular beam that traverses the spectrometer perpendicularly: $v=\sqrt{v_x^2+v_{\mathrm{beam}}^2}$. The derivatives necessary for transforming the experimental data are

$$\left|\frac{dv}{dt}\right|=\frac{s^2}{v\cdot t^3}\quad\text{resp.}\quad\left|\frac{dE}{dt}\right|=\frac{m\cdot s^2}{t^3} \qquad (A5)$$

so that the t^3 normalization for obtaining the kinetic energy spectra from drift profiles also holds for the case of nonzero velocity of the center of mass in the laboratory system

$$f_E(E)\sim t^3\cdot f_t(t). \qquad (A6)$$

[1] B. Pouilly, P. J. Dagdigian, and M. H. Alexander, J. Chem. Phys. **87**, 7118 (1987).
[2] M. N. R. Ashfold, I. R. Lambert, D. H. Mordaunt, G. P. Morley, and C. M. Western, J. Phys. Chem. **96**, 2938 (1992).
[3] G. E. Busch, J. F. Cornelius, R. T. Mahoney, R. I. Morse, and D. W. Schlosser, Rev. Sci. Instr. **41**, 1066 (1970).
[4] R. B. Bernstein and R. D. Levine, Adv. At. Mol. Phys. **11**, 215 (1975).
[5] R. D. Levine, Ann. Rev. Phys. Chem. **29**, 59 (1978).
[6] R. D. Levine, Adv. Chem. Phys. **239**, 41 (1981).
[7] C. E. M. Strauss and P. L. Houston, J. Phys. Chem. **94**, 8751 (1990).

[8] G. Baum, C. S. Effenhauser, P. Felder, and J. R. Huber, J. Phys. Chem. **96**, 756 (1992).
[9] H. Okabe, in *Photochemistry of Small Molecules* (Wiley, New York, 1978), p. 289–p. 290.
[10] D. C. Moule and P. D. Foo, J. Chem. Phys. **55**, 1262 (1971).
[11] C. B. Moore and J. C. Weisshaar, Ann. Rev. Phys. Chem. **34**, 525 (1983).
[12] W. H. Green, C. B. Moore, and W. F. Polik, Ann. Rev. Phys. Chem. **43**, 591 (1992).
[13] G. Helas and S. R. Wilson, Atmospheric Environment A **26**, 2975 (1992).
[14] S. R. Wilson, P. J. Crutzen, G. Schuster, D. W. T. Griffith, and G. Helas, Nature (London) **334**, 689 (1988).
[15] J. Heicklen, J. Am. Chem. Soc. **87**, 444 (1965).
[16] M. H. J. Wijnen, J. Am. Chem. Soc. **83**, 3014 (1961).
[17] H. Okabe, J. Chem. Phys. **66**, 258 (1977).
[18] A. I. Chichinin, Chem. Phys. Lett. **209**, 459 (1993).
[19] T. Haas, K.-H. Gericke, C. Maul, and F. J. Comes, Chem. Phys. Lett. **202**, 108 (1993).
[20] N. Arepalli, N. Presser, D. Robie, and R. Gordon, Chem. Phys. Lett. **151**, 335 (1985).
[21] Y. Matsumi, M. Kawasaki, T. Sato, Kinugawa, and T. Arikawa, Chem. Phys. Lett. **155**, 486 (1989).
[22] Y. Matsumi, K. Tonokura, and M. Kawasaki, J. Chem. Phys. **97**, 1065 (1992).
[23] Y. Matsumi, P. Kumar Das, and M. Kawasaki, J. Chem. Phys. **92**, 1696 (1990), **97**, 5261 (1992).
[24] M. Mons and I. Dimicoli, J. Chem. Phys. **90**, 4037 (1989).
[25] J. S. Francisco and A. N. Goldstein, Chem. Phys. **128**, 367 (1988).
[26] L. C. Walker and H. Prophet, Trans. Faraday Soc. **63**, 879 (1967).
[27] S. W. North, C. A. Longfellow, and Y. T. Lee, J. Chem. Phys. **99**, 4423 (1993).